NIH Public Access
Author Manuscript
Magn Reson Imaging. Author manuscript; available in PMC 2009 April 1.

Published in final edited form as:
Magn Reson Imaging. 2008 April ; 26(3): 347–359.

Relaxation Effects in the Quantification of Fat using Gradient Echo Imaging

Mark Bydder[1], **Takeshi Yokoo**[1], **Gavin Hamilton**[1], **Michael S Middleton**[1], **Alyssa D Chavez**[1], **Jeffrey B Schwimmer**[2], **Joel E Lavine**[2], and **Claude B Sirlin**[1]

1*MR3 Research Building, University of California San Diego, 408 Dickenson St, San Diego, CA 92103 - 8226*

2*Dept of Pediatrics, University of California San Diego, 200 West Arbor Drive, San Diego, CA 92103*

Abstract

Quantification of fat has been investigated using images acquired from multiple gradient echos. The evolution of the signal with echo time and flip angle was measured in phantoms of known fat and water composition and in 21 research subjects with fatty liver. Data were compared to different models of the signal equation, in which each model makes different assumptions about the T1 and/or T2* relaxation effects. A range of T1, T2*, fat fraction and number of echos was investigated to cover situations of relevance to clinical imaging. Results indicate that quantification is most accurate at low flip angles (to minimize T1 effects) with a small number of echos (to minimize spectral broadening effects). At short echo times the spectral broadening effects manifest as a short apparent T2 for the fat component.

Introduction

One of the most commonly used magnetic resonance (MR) methods for fat detection and quantification is gradient recalled echo (GRE) imaging using Dixon's 2-point technique (1). This method assumes a simplified two component system wherein the observed MR signal is the summation of two signal sources: fat protons and water protons, which are characterized by a distinct chemical shift of approximately 3.5 parts-per-million (ppm). Images are acquired at two echo times (TEs) at which the signals from fat protons and water protons are presumed to be exactly in-phase (IP) and out-of-phase (OP). Since these images are acquired with TEs that are short relative to the T2* of healthy liver (approximately 30 ms at 1.5 T), it is normally assumed that T2* decay is negligible and all signal variation between the two TEs is due to the phase interference of the fat and water protons.

Under these assumptions, the IP image is simply the sum of the water and fat signals and the OP image is the difference between the water and fat signals. The water and fat amplitudes (S_1 and S_2, respectively) can then be estimated by linear combinations of the IP and OP images.

$$S_1 \approx (\mathrm{IP} + \mathrm{OP})/2 \quad [1]$$

$$S_2 \approx (\mathrm{IP} - \mathrm{OP})/2 \quad [2]$$

Nominally it is assumed that S_1 is water and S_2 is fat although, in practice, these can only represent the "majority" and "minority" components of the signal, which is the familiar fat-

Mark Bydder, PHONE/FAX 619 471 0520/619 471 0503, EMAIL mbydder@ucsd.edu.

water ambiguity problem (2-4). Ambiguity is intimately related to B0 field homogeneity, which in turn is related to the problem of multidimensional phase unwrapping (5).

The first equation provides a means of obtaining a water only image (i.e. fat-suppression contrast) and the second a fat only image. Of particular clinical interest is the fat fraction, defined by Eq 3.

$$F = \frac{S_2}{S_1 + S_2} \quad [3]$$

When the conditions leading to Eq 1 and 2 are satisfied, the fat fraction can be estimated by rearrangement of Eq 1 and 2.

$$F_{\text{Dixon}} = \frac{\text{IP} - \text{OP}}{2\text{IP}} \quad [4]$$

The 2-point Dixon technique is clinically used as an indicator for the presence of fat although it is recognized that Eq 4 is not valid for many cases of clinical importance where T2* decay is significant (6). A regular occurrence is that the T2* decay causes signal from the later echo to be lower than the signal from the earlier echo, which leads to spurious negative values for the fat fraction when the IP image is acquired later than the OP image.

In addition to the effects of T2* relaxation, the fat fraction can be shown to be sensitive to differences in T1 relaxation (7), which introduces a dependence on imaging parameters such as repetition time (TR) and flip-angle (α). It is usually observed that the measured fat fraction increases with flip angle owing to the preferential suppression of longer T1 components. Since imaging parameters are typically optimized for signal-to-noise ratio (SNR) and/or scan time, a given protocol may induce significant T1-weighting bias in the fat fraction estimate.

As well as relaxation effects, fat is known to have a complicated chemical spectrum that contains a number of different spectral components (8): CH3, CH2, CH2COOR and CH=CH groups at 0.9, 1.2, 2.2 and 5.3 ppm, respectively, which collectively represent the total fat signal. The phase interaction between different fat components can add considerable complexity to the observed signal variation with TE especially at longer TEs.

The primary goal of this paper is to overcome the limitations of the conventional 2-point method for fat quantification. This is done by starting with a comprehensive model of the MR signal that incorporates T2* relaxation effects, B0 inhomogeneity, spectral complexity and T1 relaxation effects, and then introducing simplifications with detailed examination of the consequences and validity of each step.

Mathematical Models

Comprehensive Model

The measured complex signal S at echo time t from a sample composed of n components is a summation of the individual signals from all the components (9),

$$S(t) = \sum_{j=1}^{n} S_j \quad \exp\left(i\omega_j t\right)\exp\left(-\nu_j^* t\right)\exp\left(i\psi t\right)\exp\left(i\varphi\right) \quad [5]$$

where the individual terms are defined in Table I. Strictly, the chemical shift term ω_j depends on the field strength and should have a dependence on ψ; however ψ is typically expressed in ppm of the main field B_0 and therefore its effect on ω_j is usually negligible.

The T2* terms $\nu_j^* = \nu_j + \nu_{sys}$ contain a contribution from the T2 of the component (ν_j) which is an intrinsic property of the tissue, and the "system" (ν_{sys}), which is dependent on the imaging voxel size, susceptibility within the patient and the action of contrast agents (10,11). When ν_{sys} dominates ν_j, the T2* term ν_j^* may be approximated as ν_{sys} for all components (12).

As well as the variation with the echo time the components have a dependence on the repetition time T and flip angle α given by Eq 6 (9).

$$S_j(T,\alpha) \propto \frac{\left(1-\exp\left(-\mu_j T\right)\right)\sin\ \alpha}{1-\exp\left(-\mu_j T\right)\cos\ \alpha} \quad [6]$$

where the terms are defined in Table I. Any differences between the T1 of fat and water introduce a dependence of the estimated fat fraction on the TR and/or flip angle, which can subsequently create a dependence on the B1 field inhomogeneity. One way to mitigate T1 effects is to use a long TR and/or low flip angle so that full T1 recovery may be assumed, otherwise T1 relaxation must be taken into account.

Eq 5 and 6 provide a complete description of the MR signal $S(t,T,\alpha)$ at any TE, TR and flip angle; therefore modeling the signal variation with TE and α provides a way to estimate the components S_j and hence the fat fraction F. The fat fraction estimated in this manner is a reflection of the relative abundance of water and fat protons only and not of any MR specific parameter. A comparable modeling approach is used in the spectroscopy analysis package jMRUI (e.g. see Ref 13) to perform curve-fitting of the free induction decay signal to a generalization of Eq 5 (in which S_j is treated as a complex variable). The number of data points acquired in spectroscopy is of the order 10^3 compared to the number of unknowns $3n + 1$ and so the approach is appropriate for a reasonably large number of components n . In contrast, the number of data points acquired in imaging is typically less than 10 and therefore it is necessary to make simplifications or assume prior knowledge to reduce the number of unknowns.

Model Simplifications

In a sense, the 2-point Dixon method represents one end-point of the scale of simplification by neglecting all relaxation and assuming $n = 2$ with a fixed chemical shift separation; at the other end of the scale, Eq 5 represents the other end-point where every parameter is a potential unknown. There are many intermediate approaches that utilize only some simplifications. Ideally a set of simplifications can be identified that make the modeling approach clinically feasible yet does not compromise the accuracy of the parameter estimation; at least, over a clinically relevant range of imaging conditions. The parameter of particular interest in the present study is the fat fraction, defined by Eq 3. Ideally fat fraction measurements should exhibit insensitivity to minor system imperfections (e.g. B0/B1 inhomogeneity) and population variability (e.g. differences in relaxation rates), which have traditionally been problematic for Dixon imaging.

Amplitude: eliminate ψ and one chemical shift parameter—One way to simplify the model without compromising the accuracy is to take the amplitude of Eq 5, which gives an interferometery equation (14). The number of unknowns is reduced by two but the number of data points is reduced by a factor of two, since the real and imaginary values are replaced by a single amplitude value. However, the real and imaginary data are basically repeat measurements at the same TE and taking the amplitude is comparable to averaging these measurements to increase SNR.

A limitation of the amplitude is that it creates ambiguity between the components, making it difficult to identify S_1 with water and S_2 with fat (see Ref 5 for detailed discussion of this

problem); recent work has shown a potential way around this limitation (4). The conventional approach for resolving ambiguity is to use complex data and solve for the unknown field map, which typically involves an assumption about the smoothness of ψ. There have been many proposed solutions although at the present time field map calculation is an open problem.

If there are characteristic differences in the T1 or T2* of the components, or it can be assumed that one component is always a majority (e.g. $S_1 > S_2$), then the ambiguity may be resolved on this basis, which is a valid approach for either complex or amplitude data. All of these approaches have been used in previous studies (2,7,15). For example, the relatively short T1 of fat compared to most other tissues means the fat fraction increases with flip angle when fat is a minority but decreases when fat is a majority (15). Likewise the fat component has been reported to have a short T2* relative to liver tissue (16).

On balance there does not seem any compelling reason to prefer complex or amplitude data for fat quantification. With complex data there are more data points but more unknowns and lower SNR, plus a smoothness assumption for ψ that may add a source of error. With amplitude data there are fewer unknowns and higher SNR, but fewer data points and potential ambiguity between fat and water. For fat quantification the field map calculation is somewhatof a distraction, since it is a parameter of little clinical interest and is not essential to resolve the ambiguity when relaxation effects are considered. Thus the present study adopted the use of amplitude data.

T2* Relaxation: include T2* terms for accuracy—Although neglecting T2* terms simplifies the model significantly, the effect on quantification can be important. For simplicity, assuming a common T2* for both fat and water and an echo time difference between IP and OP of ΔTE, the fat fraction estimated by Eq 4 can be calculated to be

$$F_{\text{Dixon}} = \exp\left(\Delta\text{TE}/\text{T2}^*\right) F - \frac{\exp\left(\Delta\text{TE}/\text{T2}^*\right) - 1}{2} \quad [7]$$

This expression approaches F only as $\Delta\text{TE}/\text{T2}^*$ tends to zero. It is instructive to define a T2* amplification factor $A_2 = F_{Dixon}/F$ which for small ΔTE/T2* evaluates to

$$A_2 \rightarrow 1 - \frac{\Delta\text{TE}}{\text{T2}^*}\left(\frac{1}{2F} - 1\right) \quad [8]$$

This equation shows that the accuracy of the 2-point technique is a function of ΔTE T2* but also of F . The sign of ΔTE and size of F determine whether A_2 is greater than one, less than one or even negative. In the present study, ΔTE is positive and $F < 0.5$ so the 2-point technique always underestimates the fat fraction. For example, if ΔTE T2* = 2.3 30 then $A_2 = 0.89$ when $F = 0.2$ and $A_2 = 0.69$ when $F = 0.1$; A_2 crosses zero when $F \approx 0.04$. Although somewhat simplified, this analysis indicates that T2* relaxation can cause non- negligible errors in the fat fraction. Numerical simulations confirm that similar errors also occur when the T2* of fat and water are allowed to differ.

Chemical Shifts: eliminate chemical shift separation—Another simplification is to assume known values a priori for the chemical shifts ω_j for all the components. This is a relatively safe assumption since there is considerable literature on the composition of fat from spectroscopy (8). Spectra from an Intralipid phantom (see Methods for detail of phantom) and a fatty liver are given in Figure 1; note there is a temperature dependent shift of the water peak in the phantom compared to in vivo (17). Principally these samples contain one water peak and four fat peaks due to CH3, CH_2, CH3COOR and CH=CH. The area under each peak gives the relative abundance of that component and the broadness is a measure of the T2*. Table II gives the relative abundance and T2 of the peaks observed in Intralipid and in 21 human subjects with fatty liver. The peak at 5.3 ppm was usually obscured by the water peak and was not

reliably estimated by spectroscopy; therefore this peak was excluded from all analyses in the present study. It is understood this introduces a small error into the results but there is no easy way to account for it due to the proximity and relative insignificance next to the water peak.

When the spectral resolution is low, the different peaks can overlap and become indistinguishable from a single peak with broad line-width. This is an important concept for Dixon imaging, since the effective spectral resolution (equal to the number of acquired echos) is typically only a few points, thus the individual peaks in the range 0.8 to 2.2 ppm and 4.8 to 5.3 ppm may manifest as broad peaks. This notion of spectral broadening leading to shortened apparent T2*s was introduced in Ref (2).

Spectral Broadening: treat multi-component fat spectrum as a broad (short T2) component—The significance of spectral broadening for Dixon imaging is that a complicated system made up of multiple peaks may appear at low (spectral) resolution like a two component system with shortened effective T2*s. Whereas Ref (2) mentioned using a Gaussian line-width to represent the spectral broadening of the fat peak and assumed that the amplitude losses were relatively small, the present study simply treats fat as another component in Eq 5. This means the fat peak has a Lorentzian line-width (18), encompassing the peaks from 0.8 to 2.2 ppm, with an associated T2* decay $\exp\left(-\nu_2^* t\right)$; thus fat should exhibit a shorter T2* than expectedfrom Table I and ν_{sys}.

To illustrate the effect of spectral broadening, Figure 2A shows data from a GRE acquisition (TR 150, $\alpha = 10°$) of an Intralipid phantom and fitted curves from two models based on Eq 5: a broad peak model ($n = 2$, short fat T2*) and a composite peak model ($n = 5$, fat components defined from the data in Table I). A system component of the T2* was also included in the models. Both curves fit the data well over the range of TEs shown ($R^2 > 0.99$) and give reasonable estimates of F (19.4 % and 17.5 %); however the fitted values of decays are quite different: $\left(\nu_1^*\right)^{-1} = 116 \quad \text{ms}$ and $\left(\nu_2^*\right)^{-1} = 11.5 \quad \text{ms}$ for the broad peak model and $\nu_{sys}^{-1} = 203 \quad \text{ms}$ for the composite peak model.

Overlooking the difference in the fat fraction, the point to note from these results is that the T2* of fat in the broad peak model must be short to mimic the effect of the fat-fat interference in the composite model. Over longer time-scales the single fat peak is inadequate to describe these interactions whereas the composite peak still fits the data well, as shown in Figure 2B.

However only the short TE behavior is of interest for clinical Dixon imaging as T2* values in vivo are generally much shorter than in the phantom. Therefore in the remainder of this study, a simplified modeling approach is adopted using $n = 2$ with the understanding that a short T2* may be necessary to represent the fat component (2).

T1 Relaxation: eliminate T1 dependence by using a low flip angle—Figure 2C shows the effect of flip angle on the measured fat fraction using the broad peak model with lines showing best-fit curves of the T1 dependences given by Eq 6. Due to the shorter T1 of fat, the T1-weighted sequence tend to overestimate the fat fraction (7, 15). A T1-weighting amplification factor A_1 may be defined,

$$A_1 = \frac{F\,(\alpha = 90°)}{F} \qquad [9]$$

where $F\,(\alpha = 90°)$is the measured fat fraction at flip angle 90° and F is the true fat fraction (or T1-corrected fat fraction). The amplification factor is a complicated function of F however for short TR it approaches

$$A_1 \rightarrow \frac{\mu_2}{\mu_1 + (\mu_2 - \mu_1) F} \quad [10]$$

which has a maximum of T1(water)/T1(fat) as F tends to zero and a minimum of unity as F tends to one. Note this means lower fat fractions are more prone to overestimation by T1-weighting. The amplification factors measured from the data in Figure 2C are plotted in Figure 2D and the expected trend is over-plotted on the data. The intercept suggests the ratio T1 (water)/T1(fat) is 8.6, although the TR of 150 ms may not be short enough to give the maximum T1-weighting and so this value may be an underestimate.

To minimize T1-weighting amplification, a long TR and/or low flip angle should be used so that full T1 recovery can be assumed between successive excitations. Alternatively, T1-relaxation terms from Eq 6 should be included in the model and data points at multiple flip angles should be acquired, which permit extrapolation to $F(\alpha \rightarrow 0)$. The latter approach introduces two new variables for the T1s (μ_j) but also increases the number of data points by a factor of two or more.

Candidate models

On the basis of the previous sections, the following basic approach was adopted: two components ($n = 2$) separated by a fixed chemical shift $\omega = 2\pi/4.6$ ms and the use of amplitude data. The result is Eq 11.

$$|S(t)| = \text{sqrt}\lfloor S_1 S_1 \exp\left(-2\nu_1^* t\right) + S_2 S_2 \exp\left(-2\nu_2^* t\right) + 2 S_1 S_2 \exp\left(-\nu_1^* t - \nu_2^* t\right) \cos(\omega t) \rfloor \quad [11]$$

As noted in previous sections, this approach exhibits robustness against several confounding issues for Dixon imaging. Firstly the use of amplitude data makes the expression insensitive to B0 inhomogeneity. Secondly, the inclusion of T2* decay terms accounts for differences in the population or system. Thirdly, a low flip angle (or multiple flip angle) acquisition reduces the effects of T1-weighting and B1 inhomogeneity.

Variations on the basic approach were tested in regard to the problem of T2* decay, as given by the following models (i) to (v). In these models a low flip angle acquisition ($\alpha = 10°$) was used and in a separate model (vi) a multiple flip angle acquisition was used.

- **i.** Constraints: $\nu_j^* = 0$. Variables: S_j. This model is the basis of Eq 4 and is the standard 2-point Dixon method.
- **ii.** Constraints: $\nu_1^* = 0$, $\nu_2^* = 1/12$. Variables: S_j. This model assumes fat has an inherent decay caused by fat-fat interference that manifests as a T2 of 12 ms.
- **iii.** Constraints: $\nu_1^* = \nu_2^* = \nu_{sys}$. Variables: S_j , ν_{sys} . This model assumes a system T2* that affects water and fat equally, which has been suggested as a suitable model for short T2* environments (12).
- **iv.** Constraints: $\nu_1^* = \nu_{sys}$, $\nu_2^* = \nu_{sys} + 1/12$. Variables S_j , ν_{sys} . This model assumes a system T2* and also that fat has its own inherent T2 decay of 12 ms caused by spectral broadening (2).
- **v.** Constraints: $\nu_1^* = \nu_{sys}$, $\nu_2^* = \nu_{sys} + \nu_2$. Variables: S_j ,ν_{sys} ν_2 . This model allows water and fat to decay independently but the T2* of fat is constrained to be shorter than water.
- **vi.** Identical to model (v) but with T1 terms included. This model allows water and fat to undergo T1 and T2* relaxation independently by modeling the signal variation with TE and flip angle.

The value 12 ms used in models (ii) and (iv) was not a random choice but was empirically derived from preliminary analyses using models (v) and (vi), which showed that the observed T2* of fat was often considerably shorter than that of water. This represents the spectral broadening of the fat peak and a value $\nu_2 = 12$ ms is tentatively suggested, although a range may be more appropriate to allow for variability in the fat spectrum. This situation is covered separately by model (v).

Materials and Methods

The accuracy of the six candidate models was tested on phantom and in vivo data. In the analysis of phantom data, the known composition of the fat-water mixtures provided a reference standard with which to compare the estimated fat fractions. In the analysis of in vivo data, where the actual fat content is not known, the fat fractions determined by MR spectroscopy were used as a reference standard.

Phantom Construction

A phantom was created in 55 ml plastic vials using distilled water and a fat emulsion Intralipid (Baxter Healthcare Corporation, Deerfield IL) in seven dilutions. Intralipid is an intravenously administered nutritional supplement containing known amount of soybean oil suspended in water by trace amount of lethicin. The labeled fat content of Intralipid is 20 % soybean oil by weight whereas MR techniques measure fat content by proton density. Taking into account the known lipid composition of soybean oil, the fat fraction by proton density of Intralipid was calculated to be 21 % (all fat peaks), 20 % (excluding CH=CH) or 17 % (CH2 peak only). Since CH=CH was excluded from all analyses due to its proximity to the water peak, the middle measure was considered the most appropriate. Therefore the fat fraction of Intralipid was taken to be 20 % by proton density.

The seven Intralipid dilutions were 20.0, 14.9, 9.8, 4.7, 2.5, 1.1 and 0 % fat fraction by proton density. To assess the sensitivity of the models to changes in T1 and T2* two additional sets of the dilutions were created by adding 25 μl of a gadolinium T1 shortening agent (Multihance, Bracco Diagnostics Inc, Princeton NJ) or 100 μl of a ferumoxides T2* shortening agent (Feridex, Berlex Imaging, Montville NJ). All three sets of these vials were immersed in a water bath containing sodium chloride solution to reduce susceptibility and load the coils.

Research Subjects

The human subject component of this study was compliant to the Health Insurance Portability and Accountability Act and was approved by the investigational review board (IRB). In accordance to the IRB protocol, institutional liver clinic recruited individuals with known or suspected non-alcoholic fatty liver disease (NAFLD) for research MR examination at the Radiology department. Informed consents were obtained prior to imaging for involvement in the research study. A total of 21 subjects were recruited: six from the Nonalcoholic Steatohepatitis Clinical Research Network (NASH CRN), and 15 from the local pediatric hospital. The age range of the subjects was 8 to 66 years with mean 27.4 years. An additional subject (female, age 50) was scanned during ferumoxides infusion given for clinical purposes.

MR Examination

Data were acquired on a Siemens Symphony Quantum 1.5T scanner using a multiple echo spoiled GRE sequence capable of sampling on the forward and reverse gradients (19). Up to 16 TEs were acquired in a single TR with minimum TE 2.3 ms and interecho spacing 2.3 ms. The TR was either 150 ms (phantom) or 122 ms (in vivo) and flip angles were in the range 10 to 90°. A bandwidth of 500 Hz/pixel was used so that the chemical shift of CH2 was less than

half a pixel. The matrix size was approximately 256×192, field of view 350×240mm and slice thickness 8 mm.

Single voxel spectroscopy was performed using the Stimulated Echo Acquisition Mode (STEAM) sequence on a 10×10×10 mm^3 voxel, 4 averages, 4 preparation pulses, bandwidth 1000 Hz, TR 3000 ms and TE 20 to 70 ms by increment of 10 ms to permit correction for T2 decay.

Phantom experiments were performed with a birdcage head coil and in vivo examinations were performed using a phased array body coil. All in vivo examinations were performed with a breath-hold protocol (less than 30 seconds). Amplitude images and raw spectroscopy files were transferred offline for processing in MATLAB (The Mathworks, MA) and jMRUI (13), respectively.

Data Analysis

Preliminary tests indicated the simplex algorithm (20) was adequate for models (i) to (iv) but not model (v) and (vi), where the results depended on the initial estimates. It was decided to do all curve-fitting with MATLAB's *lsqcurvefit* function, which is based on the interior-reflective Newton method described in Ref (21,22) This approach was reliable for all models using the following fitting parameters: tolerance ("TolFun") 10^{-12}, maximum number of iterations ("MaxIter") 2000, maximum function evaluations ("MaxFunEvals") 10000, maximum preconditioned conjugate gradient iterations ("MaxPCGIter") 1. Bound constraints $1/5000 \leq \mu_j \leq 1/50$ and $1/500 \leq v_j$, $v_{sys} \leq 5$ were used to prevent $\mu_j \rightarrow \infty$ or $v_j \rightarrow \infty$, which remained problematic for the optimization algorithm (since the fitted signal became zero before the first data point).

Although the primary goal was to determine the fat fraction, the data analysis also provided relaxation constants for the components in the model. Caution must be heeded in interpreting the fitted values since T1s obtained by varying the flip angle are partly a measure of the B1 field homogeneity and may be inaccurate compared to other methods (23). Similarly, T2*s depend on spectral broadening, susceptibility and diffusion effects (2). The T1 values of liver tissue and fat were expected to be around 490 ms and 260 ms, respectively, (24) and the T2* values around 30 ms and 10 ms (16).

Results

Phantom Study

Figure 3 shows results from the phantom experiment. Seven dilutions of Intralipid were used: ferumoxides-doped (left column), non-doped (center column) and gadolinium-doped (right column). The signal variation with TE exhibits the phase interference between fat and water and also relaxation effects, which may include contrast agent doping.

The true fat fractions were 20.0, 14.9, 9.8, 4.7, 2.5, 1.1 and 0 %. For comparison, the spectroscopy estimates (using fat peaks in the range 0.8 to 2.2 ppm) were 22.2, 19.2, 11.4, 5.2, 2.6, 0.7 and 0 %. The minimum voxel size of 10×10×10 mm^3 meant that susceptibility dephasing from to the plastic of the container occurred inside the spectroscopy voxel, which was not ideal for obtaining high quality spectra. Nevertheless, the spectroscopy fat fractions are in general agreement with the known fat composition.

Panels (A) - (F) show the fat fractions determined by models (i) - (vi) using the first five echos. The images are windowed identically so the rows should appear iso-intense. Clearly models (i) and (ii) underestimate the fat fraction in the ferumoxides doped mixtures while models (iii)

to (vi) appear to be give similar estimates along the rows. The accuracy of all the models is assessed quantitatively in Figure 4.

Figure 4 shows a plot of the estimated fat fractions for each model in the three environments: gadolinium-doped (panel A), non-doped (panel B) and ferumoxides-doped (panel C). To reduce noise scatter the median within a region of interest at the center of each vial was used (containing approximately 50 pixels). The median was preferred over the mean due to outliers, which sometimes occurred in the fitted values due to acute sensitivity to small variations in the data. This is a problem with all curve-fitting methods when there are a large number of free parameters compared to the number of data points because the algorithm tries to fit the noise variation and the fitted values are spurious. The present study has no solution to this problem but notes that it must be a consideration in the choice of model as well as the quantification accuracy.

Table III shows the median values of the T2* parameters estimated by each model. The results of models (v) and (vi), which allow the T2* of fat and water to change independently, indicate there is a significant difference in the estimated T2* values of fat and water. The median T1 values determined from model (vi) are also given in Table III. The accuracy of the T1 estimates depends on the calibration of the flip angle and B1 inhomogeneity and hence may be inaccurate by a scaling; nevertheless, fitting removes the trend and so the estimated fat fraction should be unaffected. Note the ratio T1(water)/T1(fat) is 11.0, which is reasonably consistent with the value 8.6 determined from Figure 2D.

The results in Figure 4 were obtained using a fixed number of echos however some of the methods may perform better with a greater or lesser number of echos. Figure 5 shows a plot of the error in the median fat fraction as a function of the number of TEs used in the fitting. Error was defined as the square root of the mean square difference between the estimated and known fat fractions in the 21 mixtures.

$$\text{Error} = sqrt\left(\frac{1}{21}\sum_{j=1}^{21}\left(F_j - F_{\text{known}}\right)^2\right) \quad [12]$$

The *Error* gives a measure of the confidence in the estimate of *F* over the range of conditions (e.g. T1, T2* and fat fraction variation). Since the *Error* effectively represents a standard deviation, the 96% confidence interval for the estimated fat fraction is ± 2 *Error* and this may be interpreted as the expected deviation from the true fat fraction.

The *Error* plot indicates a correlation between the sophistication of the model and the accuracy of the fat fraction estimate. It also shows that the *Error* tends to increase with number of TEs, which is likely due to the failure of the two component models to capture complicated interference effects at longer echo times (e.g. Figure 2B). Based on Figure 5, the most accurate method for determining the fat fraction is model (vi) using 4 echos with an *Error* of 0.6 %. This model requires the acquisition of multiple flip angles, which has two advantages: noise is reduced due to the larger number of data points and T1 effects are fully corrected. Models (iv) and (v) have the next best accuracy using between four and six echos, with *Errors* of around 1.8 %, although these rely on minimizing T1 effects by using a flip angle of 10°.

When deciding upon which model to implement for online reconstruction, there are practical concerns to consider as well as quantification accuracy. Such concerns include scanner stability (e.g. flip angle calibration) and potential mis-registration between scans, as well as the familiar issues from curve-fitting of computation time, reliability and noise performance. The first set of problems are only applicable to model (vi), which requires multiple flip angle acquisitions

and hence may require efforts to ensure B1 field homogeneity and image registration for imaging in vivo.

The second set of problems are generally improved when there are fewer free parameters in the model or more acquired data points. Since the long TE behavior of the signal is complicated by the spectral complexity of fat, the number of data points is effectively limited by the number of TEs that can be acquired within two to three periods of the fat-water oscillation cycle. Within this constraint model (v) is more accurate but, as noted in Methods and from the fat fraction maps in Figure 3, the fitting is computationally more demanding and the noise-performance is worse. Thus the present study has opted to implement model (iv) for online reconstruction as a compromise between practical reconstruction and quantification accuracy over the conditions studied.

In Vivo Study

Figure 6 shows results obtained from model (iv) using the online reconstruction in a fatty liver patient before, during and after ferumoxides infusion, which occurred over a period of approximately 30 minutes. For comparison, panels A and B show the before and after fat fractions from model (i) using two echos only (i.e. 2-point Dixon) and panels C and D show the before and after fat fractions determined from model (iv) using six echos. Note panels A-D are windowed and leveled identically. The median values inside a region-of-interest (ROI) drawn in the liver (shown in A) are 17.4 & 13.9 % for A & B, which indicates the T2* shortening of ferumoxides has caused a decrease in the estimated fat fraction, while values in the same ROI in C & D are 24.6 & 25.7 %, which shows the fat fraction is not sensitive to the T2*. The higher value for the pre-ferumoxides data (i.e. 24.6 compared to 17.4) is likely due to the short apparent T2 of fat $\left(\nu_2^{-1}\right)$ of around 12 ms that is neglected by model (i). Panels E and F show the T2* estimates of the system ν_{sys}^{-1} by model (iv), which are 24.6 and 9.8 ms, respectively.

Evidently in the fat fraction maps, subcutaneous fat is not correctly assigned since the fat fraction should approach one in these tissues. Model (iv) assumes there are two components and that the fat component has the shorter T2*; however a problem is that even pure fat contains multiple components and can give an oscillatory signal (25). The oscillation is incorrectly identified as fat-water interference and the component with the shorter T2* will be identified as fat. In these tissues, fat fraction maps are a measure of the relative proportions of the fat peaks rather than the water peak.

Figure 7 shows plots of the signal in an ROI inside the liver at different times during the ferumoxides infusion. Best fit curves to model (iv) are over-plotted on the data. Fitted values to model (i) (using two echos only), and models (iii) to (v) (using all six echos) are given in Table IV. The results indicate that models (i) and (iii) underestimate the fat fraction compared to models (iv) and (v) and that models (iii) - (v) are not sensitive to the T2* agent, as might be expected since T2* terms are included. Unfortunately spectroscopy was not performed on this patient; however the results are entirely consistent with the phantom data of Figure 4, which indicated that models (i) and (iii) underestimate the fat fraction.

At higher ferumoxides concentrations the plot of signal versus TE takes on a “staircase” appearance, where adjacent OP and IP images have equal intensities and so the 2-point Dixon method (Eq 4) approaches a zero fat fraction. At still higher ferumoxides concentrations the 2-point method gives negative fat fractions, as expected from Eq 8. In this subject the system T2* reached a minimum of 9 ms and the fat fraction from the 2-point method was approximately half the corrected value. In clinical imaging it is not uncommon to observe subjects who have more severely shortened T2* due to iron overload and consequently a negative fat fraction, although such results were not included in the present study.

Figure 8 shows the in vivo fat fractions in 21 research subjects as determined by models (iv) and (v) (circle and square markers, respectively) and by spectroscopy. As noted above, for spectroscopy the fat component was defined to be the sum of all peaks in the range 0.8 to 2.2 ppm. Panels A and B show, respectively, results for the lowest and highest flip angles (10° and 90°). The latter exhibits stronger T1-weighting and so the measured fat fractions are overestimated with respect to the spectroscopy results, which used a much longer TR. The lines overplotted on the data give the theoretical trends assuming literature values for the T1s (24); note that linearity is only obtained when the T1-weighting is minimized, since low fat fraction data points tend to be more overestimated than high fat fraction data points (e.g. see Figure 2d). Fitting a linear trend to these data would give rise to an erroneous intercept.

Assuming spectroscopy gives the true fat fraction (F_{known}), the *Error* defined by Eq 12 can be calculated for each model and is given in Table V. The results show model (i) is least accurate method and model (v) is the most accurate. For model (vi), regions of interest were manually defined in approximately the same location for each flip angle as these required separate breath-hold acquisitions. This may explain the poorer accuracy of the in vivo results compared to the phantom (Figure 5). Otherwise the results are broadly consistent with those obtained in the phantom.

Discussion

Quantification of fat has been a long-standing topic of interest in MR imaging that has received renewed attention owing, in part, to the rise in incidence of NAFLD with obesity in developed nations (26). Previous studies have recognized several factors that interfere with accurate quantification; notably B0 field homogeneity, fat/water ambiguity, noise performance, T1-weighting (flip angle, B1 homogeneity) and T2*-weighting (iron deposition, spectral broadening). Whereas significant advances have been made in modeling B0 homogeneity and optimizing noise performance, the assessment of accuracy of the fat fraction estimates with respect to relaxation parameters has received comparatively less attention.

Relaxation

Recent work has shown that rapid T2* relaxation caused by iron-overload in the liver is a confounding factor in estimating fat fraction using 2-point Dixon methods (c.f. Eq 4) (6). The analysis of the present study indicates that this method underestimates fat fraction in a manner that depends on the T2* and also the fat fraction. A T2*-weighting amplification factor A_2 can be defined (e.g. Eq 8) to estimate the degree of underestimation. Experimental results confirm that the 2-point method is less accurate than other, more sophisticated, methods that account partly or fully for the T2* losses.

The T1 results in Figure 2C compare to the work of Ref (7), where negative fat fractions were obtained in some experiments and a flip angle of 30° - 50° was found to be necessary to obtain agreement with the known composition. Ref (7) noted that the effects of T1 and T2* relaxation on *F* were, respectively, underestimation and overestimation (since the T1 and T2* of fat are both short relative to water) and the approach was a pragmatic attempt to balance the two errors. If a T1-weighting amplification factor A_1 is defined (e.g. Eq 9), then the basic approach is to ensure $A_1A_2 = 1$; substituting for A_1 and A_2 produces an expression that indicates particular combinations of TR, flip angle and T2* may satisfy the equality. However, the approach of the present study has been to ensure $A_1 = 1$ by using a low flip angle and properly account for T2* relaxation by modeling.

Results from modeling indicate that the T2* values of water and fat are different. A previous study (2) reported that spectral broadening of fat should give rise to a shorter apparent T2 for fat and this effect is confirmed in the present study and has also been observed in previous

work (16). Assigning a value for the T2 is somewhat problematic since it depends on the fat spectrum, which may differ from patient to patient and also with field strength. A tentative value of 12 ms is suggested, based on results from the present study which were obtained at 1.5 T. At higher field strength the increased spectral separation may lead to values that scale with B0 and so signal decay may remain a problem despite the closer IP and OP echo spacing.

The T2* for fat in fat-water mixtures has previously been estimated in various ways, such as by curve-fitting a mono-exponential decay to the IP and/or OP data points. It is unclear what the values from such an analysis represent, since a bi-exponential decay would seem to be necessary for two components. Results from the present study suggest that neither IP nor OP data points follow a mono-exponential decay (Figure 2B). At longer echo times it does not seem possible to obtain satisfactory agreement between the model and the data except using a multi-component model to represent the fat spectrum. Simplifying the fat to a single component appears to be valid only in the limit of short echo times, which corresponds to low spectral resolution.

Ambiguity

Fat-water ambiguity is inextricably linked with B0 homogeneity, which is an area of active research in MR imaging (e.g. 27,28). Although correcting B0 homogeneity with an automated algorithm is non-trivial, for the radiologist it may be relatively easy to identify tissues where the fat fraction is incorrectly assigned. The present study has relied upon a distinctive short T2 of fat compared to water to resolve ambiguity, which appears to be adequate in areas where the fat fraction is up to 50 % but may be inaccurate or ambiguous outside these ranges.

Clearly the perfect method should be able to provide high accuracy in all cases, however a problem is when the fat fraction exceeds a certain percentage (e.g. in adipose tissue) the size of the water peak becomes comparable to the minor components of the fat spectrum. It is somewhat arbitrary to neglect those components while still retaining the water component, especially when the observed interference phenomena are primarily due to fat-fat rather than fat-water. Thus it may be hard to quantify fat accurately above a certain percentage using a model that assumes only two components. Using a model that assumes a composite fat peak made up of several components can help capture some of the subtleties in the signal variation (e.g. see Figure 2B) and may provide a way of resolving fat/water ambiguity since the fat and water components no longer have the same basis function (25).

Noise

It may be verified from Figure 3 that the noise in the fat fraction depends on the number of free parameters in the model compared to the number of data points. The noise error also depends on the fat fraction and the choice of echo times (29) while the systematic error depends primarily on the choice of model (see Figure 4). It is not necessarily the case that protocols that minimize the noise error coincide with those that minimize the systematic error. In particular, the noise error is minimized with a high flip angle (the Ernst angle) and the systematic error is minimized with a low flip angle. A comparable situation is observed with the number of echos, where increasing the number of echos can reduce noise but also reduces the accuracy due to a breakdown in the assumptions of the model (see Figure 4).

A minor point regarding noise is that amplitude images exhibit a Rician distribution rather than Gaussian, which has the effect of elevating the noise floor. The effect is insignificant except at extremely low SNR (say, less than 5) as long as the coil images are combined optimally, which was the case in the present study (30).

Conclusion

The present study has assessed T1 and T2* relaxation effects in the quantification of fat by comparing several models of the signal variation with flip angle and TE. It is possible to obtain accurate quantification over a range of fat fractions, T1 and T2* that is relevant to the clinical imaging of the liver.

Acknowledgements

This work was performed as an ancillary study (#AS009) of the Nonalcoholic Steatohepatitis Clinical Research Network (NASH CRN). The NASH CRN is supported by the National Institute of Diabetes and Digestive and Kidney Diseases (NIDDK) (UCSD #1U01DK061734, Data Coordinating Center #5U01DK061730) and the National Institute of Child Health and Human Development (NICHD). Funding was provided by NIH grant R01 (#DK075128).

References

1. Dixon WT. Simple Proton Spectroscopic Imaging. Radiology 1984;153:189. [PubMed: 6089263]
2. Glover GH. Multipoint Dixon Technique for Water and Fat Proton and Susceptibility Imaging. J Magn Reson Imag 1991;1:521.
3. Yeung HN, Kormos DW. Separation of true fat and water images by correcting magnetic field inhomogeneity in situ. Radiology 1986;159:783. [PubMed: 3704157]
4. Xiang QS. Two-point water-fat imaging with partially-opposed-phase (POP) acquisition: an asymmetric Dixon method. Magn Reson Med 2006;56:572. [PubMed: 16894578]
5. Pauly, J. Course notes on 'Dixon Reconstruction'. http://www.stanford.edu/class/ee369c/notes/dixon.pdf
6. Westphalen ACA, Qayyum A, Yeh BM, Merriman RB, Lee JA, Lamba A, Lu Y, Coakley FV. Liver Fat: Effect of Hepatic Iron Deposition on Evaluation with Opposed-Phase MR Imaging. Radiology 2007;242:450. [PubMed: 17255416]
7. Fishbein MH, Gardner KG, Potter CJ, Schmalbrock P, Smith MA. Introduction of Fast MR Imaging in the Assessment of Hepatic Steatosis. Magn Reson Imaging 1997;15:287. [PubMed: 9201675]
8. Fauhl C, Reniero F, Guillou C. 1H NMR as a tool for the analysis of mixtures of virgin olive oil with oils of different botanical origin. Magn. Reson. Chem 2000;38:436.
9. McRobbie, DW.; Moore, EA.; Graves, MJ.; Prince, MR. MRI From Picture to Proton. Cambridge University Press; 2003. p. 240
10. Bernstein, MA.; King, KF.; Zhou, XJ. Handbook of MRI Pulse Sequences. Elsevier Academic Press; 2004. p. 581
11. McRobbie, DW.; Moore, EA.; Graves, MJ.; Prince, MR. MRI From Picture to Proton. Cambridge University Press; 2003. p. 162
12. Yu H, McKenzie CA, Shimakawa A, Pelc NJ, Brittain JH, Reeder SB. IDEAL Water- Fat Separation with Simultaneous T2* Estimation. Proc ISMRM 2006:624.
13. Vanhamme L, van den Boogaart A, Van Huffel S. Improved Method for Accurate and Efficient Quantification of MRS Data with Use of Prior Knowledge. J Magn Res 1997;129:35.
14. Ford JC, Wehrli FW. In Vivo Quantitative Characterization of Trabecular Bone by NMR Interferometery and Localized Proton Spectroscopy. Magn Reson Med 1991;17:543. [PubMed: 1648162]
15. Hussain HK, Chenevert TL, Londy FJ, Gulani V, Swanson SD, McKenna BJ, Appelman HD, Adusumilli S, Greenson JK, Conjeevaram HS. Hepatic Fat Fraction: MR Imaging for Quantitative Measurement and Display—Early Experience. Radiology 2005;237:1048–1055. [PubMed: 16237138]
16. Bydder M, Middleton MS, Gatehouse PD, Chavez AD, Sirlin CB. Fat quantification by modeling the variation in signal amplitude with TE. Proc ISMRM 2006:2298.
17. Kuroda, K.; Tsutsumi, S.; Chapter, C. NMR tomography II: Temperature imaging by proton chemical shift. In: Miyakawa, MBJ., editor. Non-invasive thermometry of the human body. CRC Press Inc; Boca Raton, FL: 1996. p. 63

18. Bernstein, MA.; King, KF.; Zhou, XJ. Handbook of MRI Pulse Sequences. Elsevier Academic Press; 2004. p. 12
19. Westwood WA, Anderson LJ, Firmin DN, Gatehouse PD, Lorenz CH, Wonke B, Pennell DJ. Interscanner reproducibility of cardiovascular magnetic resonance T2* measurements of tissue iron in thalassemia. J Magn Reson Imaging 2003;18:616. [PubMed: 14579406]
20. Press, WH.; Teukolsky, SA.; Vetterling, WT.; Flannery, BP. Numerical Recipes in C. 2nd ed.. Cambridge University Press; Cambridge: 1992. p. 408
21. Coleman TF, Li Y. On the Convergence of Reflective Newton Methods for Large- Scale Nonlinear Minimization Subject to Bounds. Mathematical Programming 1994;67:189.
22. Coleman TF, Li Y. An Interior, Trust Region Approach for Nonlinear Minimization Subject to Bounds. SIAM Journal on Optimization 1996;6:418.
23. Venkatesan R, Lin W, Haacke EM. Accurate determination of spin density and T1 in the presence of RF-field inhomogeneities and flip angle miscalibration. Magn Reson Med 1998;40:592. [PubMed: 9771576]
24. Bernstein, MA.; King, KF.; Zhou, XJ. Handbook of MRI Pulse Sequences. Elsevier Academic Press; 2004. p. 961
25. Bydder M, Hamilton G, Yokoo T, Middleton MS, Chavez AD, Sirlin CB. Fat-Fat Interactions in Dixon-Variant Imaging. Proc ISMRM 2007:1632.
26. Patton HM, Sirlin CB, Behling C, Middleton MS, Schwimmer JB, Lavine JE. Pediatric Nonalcoholic Fatty Liver Disease: A Critical Appraisal of Current Data and Implications for Future Research. Journal of Pediatric Gastroenterology and Nutrition 2006;42:4. [PubMed: 16385244]
27. Ma J. Breath-Hold Water and Fat Imaging Using a Dual-Echo Two-Point Dixon Technique With an Efficient and Robust Phase-Correction Algorithm. Magn Reson Med 2004;52:415. [PubMed: 15282827]
28. Reeder SB, Wen Z, Yu H, Pineda AR, Gold GE, Markl M, Pelc NJ. Multicoil Dixon chemical species separation with an iterative least squares estimation method. Magn Reson Med 2004;51:35. [PubMed: 14705043]
29. Pineda AR, Reeder SB, Wen Z, Pelc NJ. Cramer-Rao bounds for three-point decomposition of water and fat. Magn Reson Med 2005;54:625. [PubMed: 16092102]
30. Bydder M, Larkman DJ, Hajnal JV. Combination of signals from array coils using image-based estimation of coil sensitivity profiles. Magn Reson Med 2002;47:539. [PubMed: 11870841]

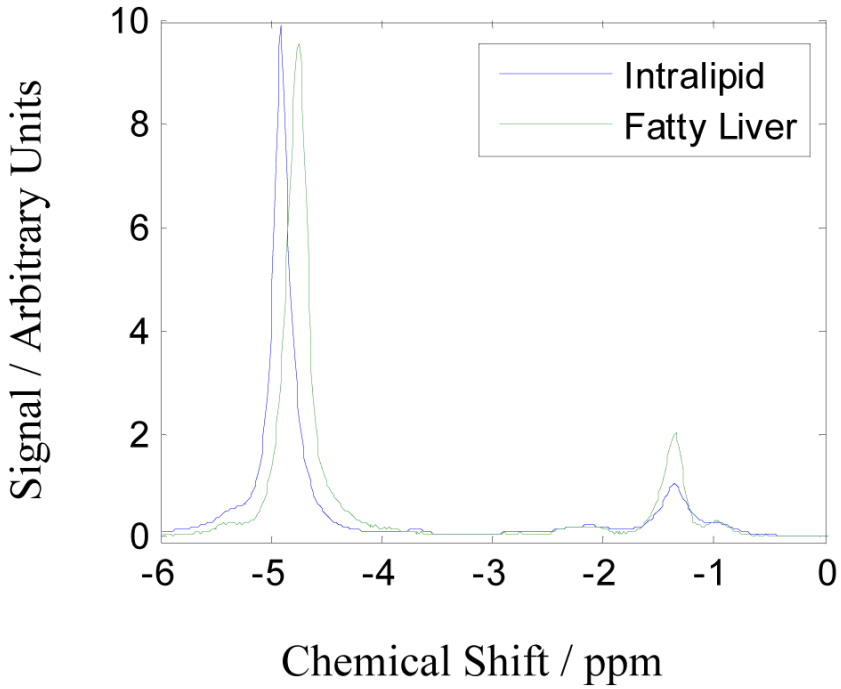

Figure 1.
MR spectra of Intralipid (solid line) and fatty liver (dashed line) taken with TR 1500 ms and TE 20 ms. The water peak (near 4.8 ppm) in Intralipid is shifted relative to the fat peak (near 1.2 ppm) due to the temperature difference of approximately 20°C between the phantom and the in vivo samples.

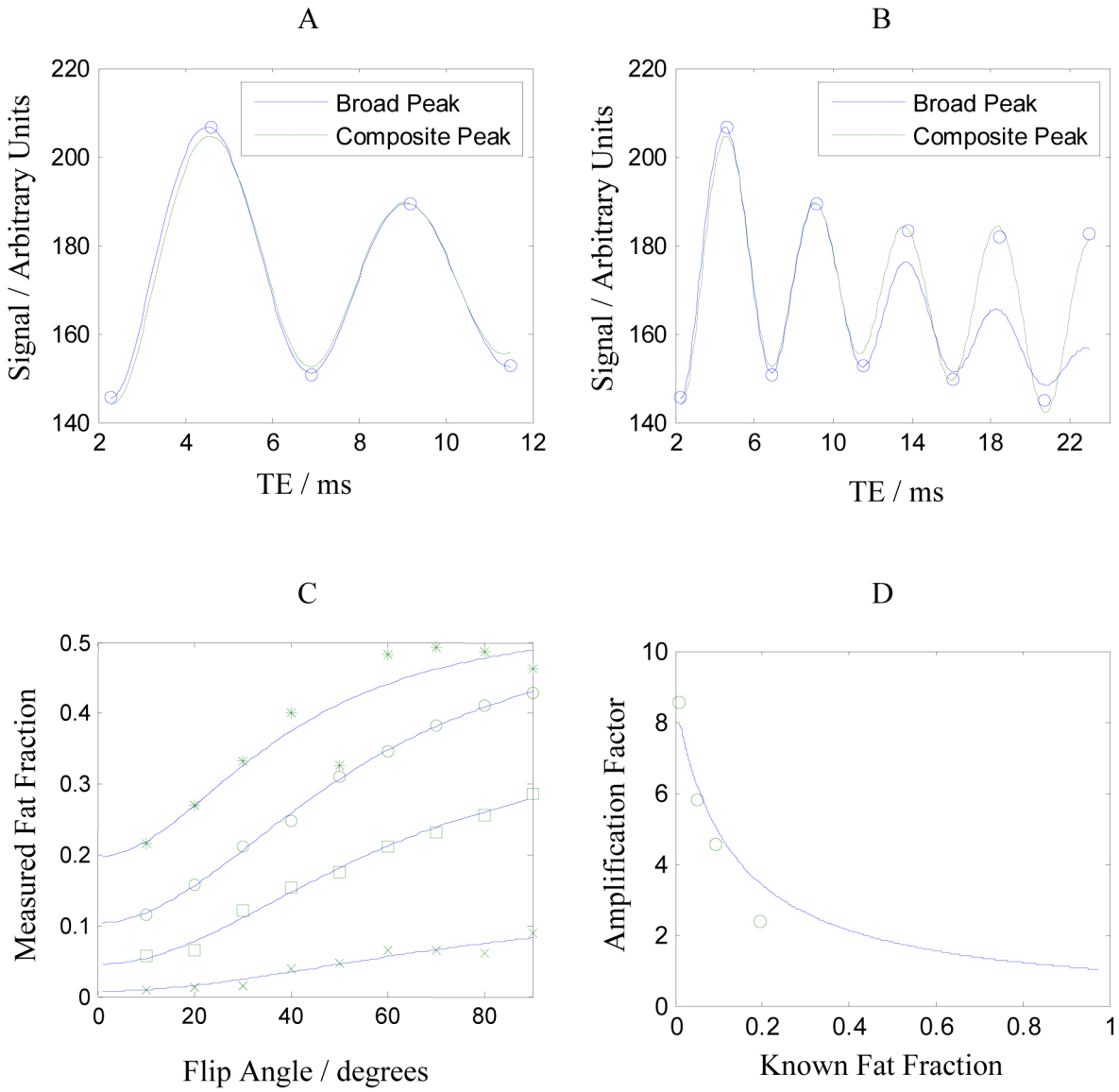

Figure 2.

Panel A shows a plot of data acquired from Intralipid over the TE range 2.3 to 11.5 ms. Best-fit curves to two models are shown, as described in the text: a broad fat peak containing two components (solid line) and a composite peak containing five components (dashed line). Panel B shows the same data set over a longer range of TE and best-fit curves to the two models. Panel C shows the 1%, 5%, 10% and 20% fat fractions estimated at different flip angles; overlaid are best-fit curves to the expected dependence due to T1 effects. Panel D shows the amplification factor A_1 (defined in Eq 9) and the best-fit curve to the data points.

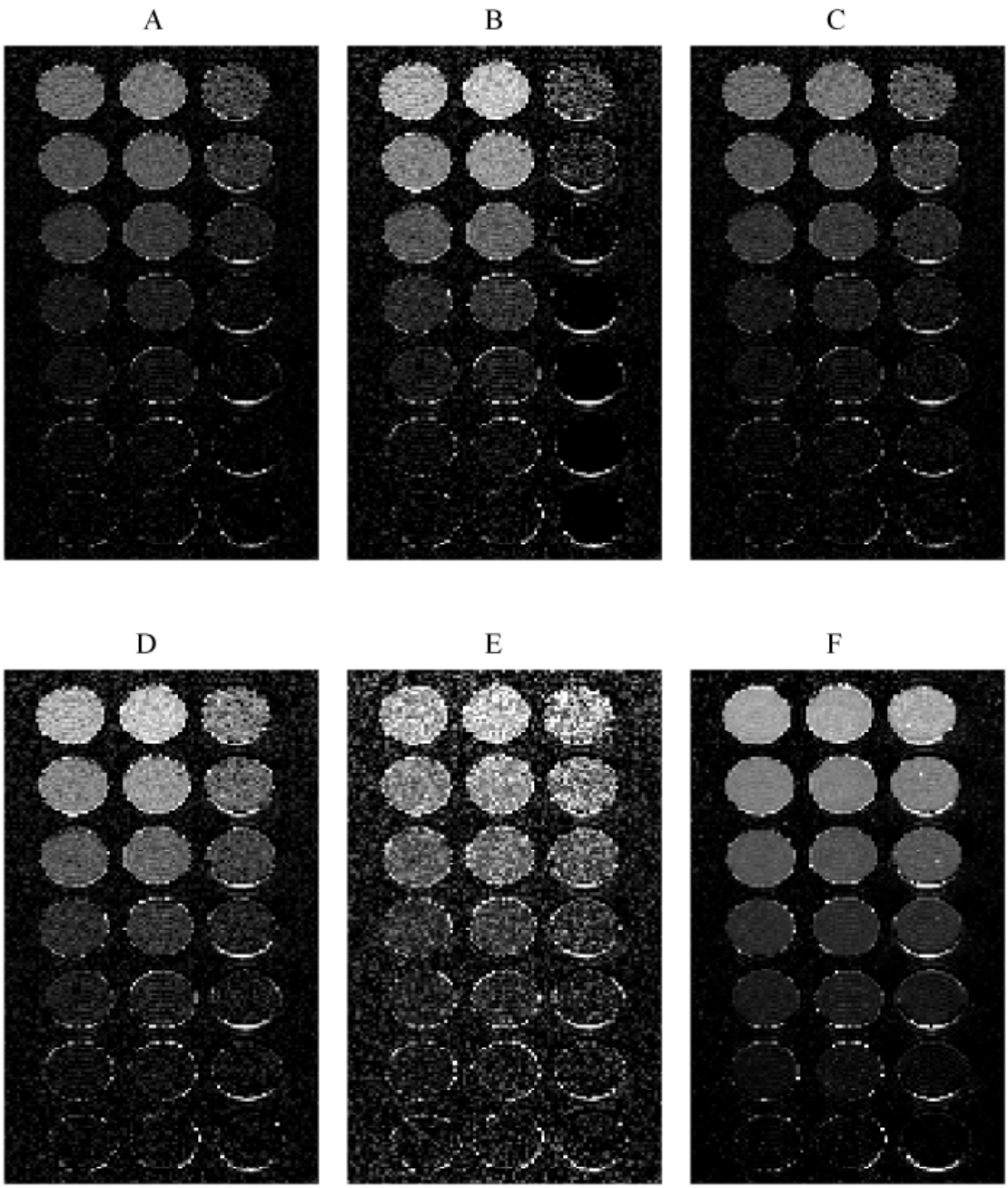

Figure 3.

Panels (A) to (F) show fat fraction maps estimated using models (i) to (vi). Columns were doped with gadolinium (left), no agent (middle) and ferumoxides (right). The known fat fractions are 20.0, 14.9, 9.8, 4.7, 2.5, 1.1 and 0 %. The images are windowed identically between 0 and 30% therefore the rows should appear iso-intense.

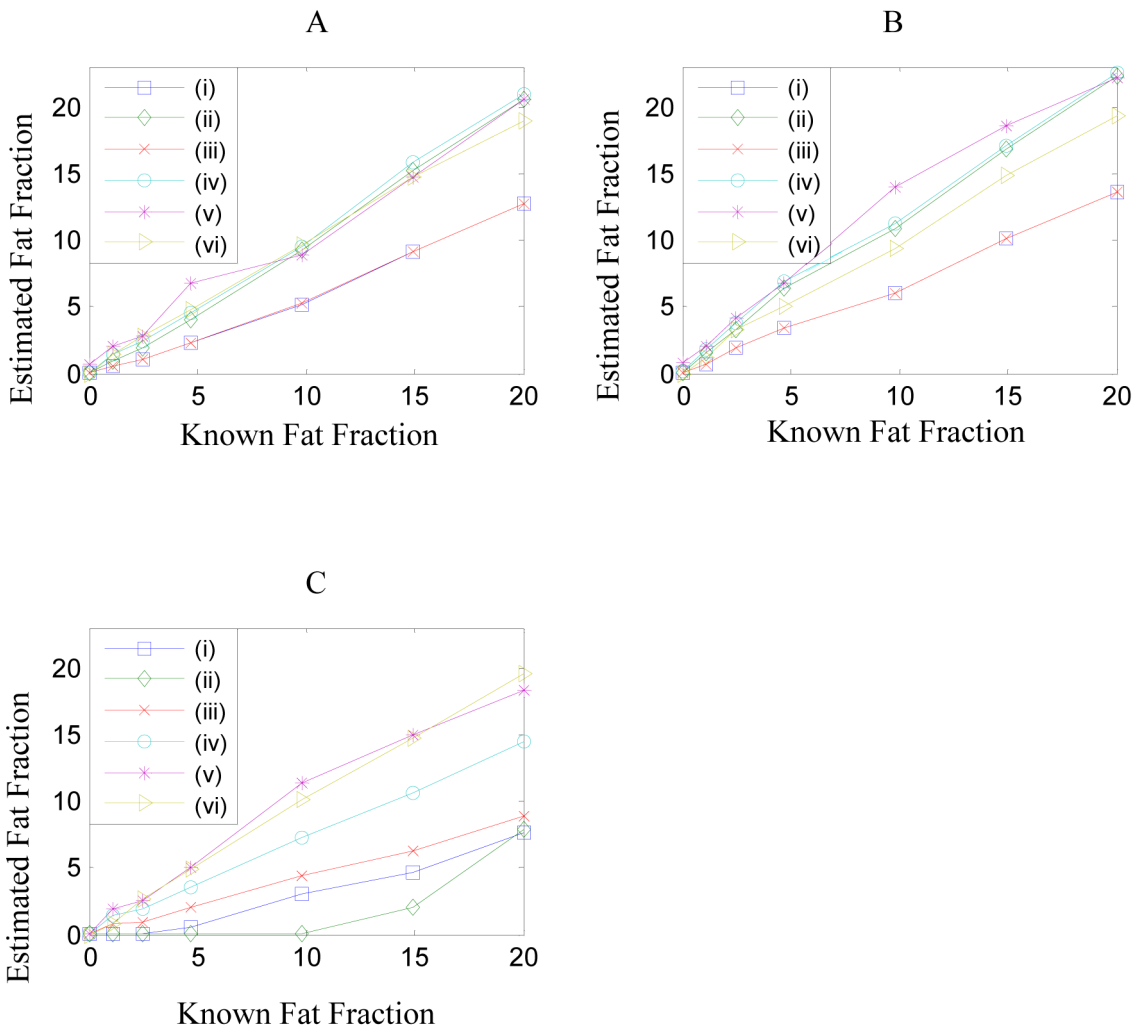

Figure 4.

The median fat fractions in the center of each vial from Figure 3 are plotted against the known fat fraction for the three doping conditions, seven dilutions and six models. Panel (A) shows the fat fractions in Gd-doped vials. Panel (B) shows the fat fractions in undoped vials. Panel (C) shows the fat fraction in Fe-doped vials. Relaxation values from the different models are given in Table III.

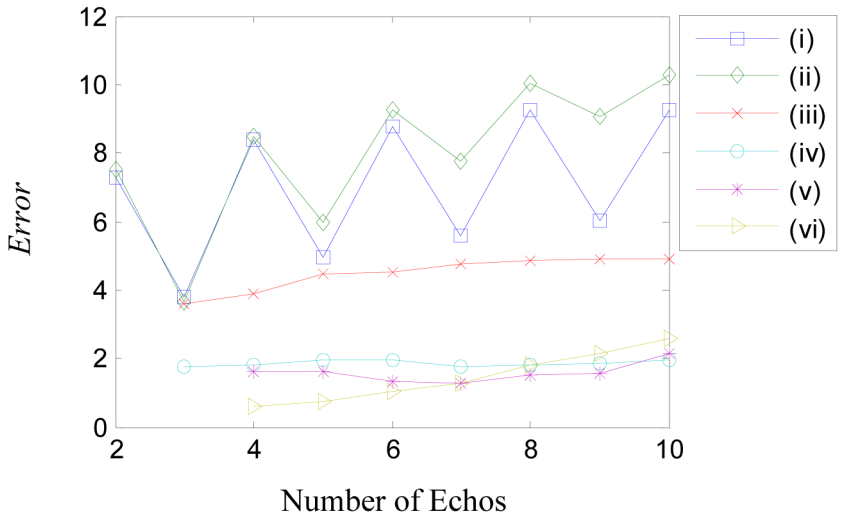

Figure 5.
Error (calculated by Eq 12) for the six models as a function of the number of data points (echos) used in the curve-fitting. Echos were added by including a later echo time acquisition therefore the *Error* is largely a measure of the breakdown in the assumption of two components at long echo times (e.g. see Figure 2B). The plots in Figure 4 correspond to the use of five echos in this plot.

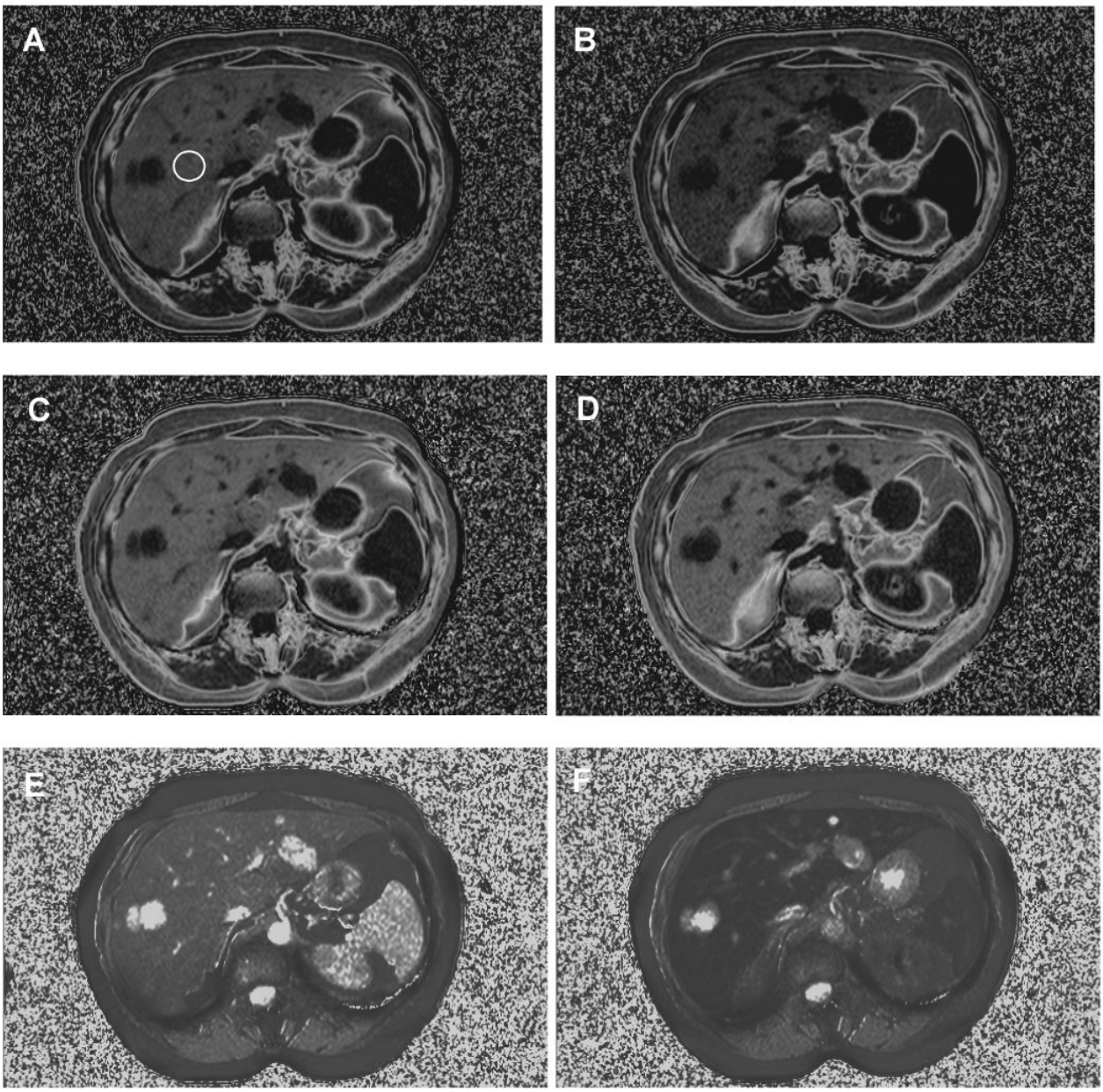

Figure 6.
In vivo fat fraction and T2* maps from a research subject who was scanned at five minute intervals during the infusion of a T2* contrast agent. Panels (A) and (B) show fat fraction maps obtained by model (i) with two echos (i.e. 2-point Dixon) at the start and end of the infusion (corresponding with the minimum and maximum contrast agent effect). There is a noticeable drop in the fat fraction (17.4 to 13.9 %). Panels (C) and (D) show the same data processed using model (iv), in which the fat fraction is relatively stable (24.6 to 25.7 %). Panels (E) and (F) show the T2* maps determined from model (iv) for the same data.

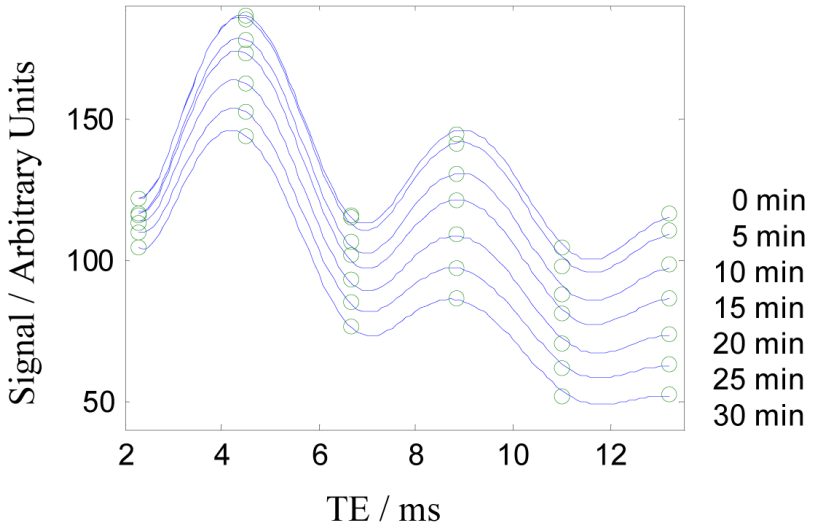

Figure 7.
Plots of the signal intensity in the liver (taken from the ROI from Figure 6) at different times during the infusion of T2* contrast agent. Best-fit curves to model (iv) are shown and the fitted values are given in Table IV.

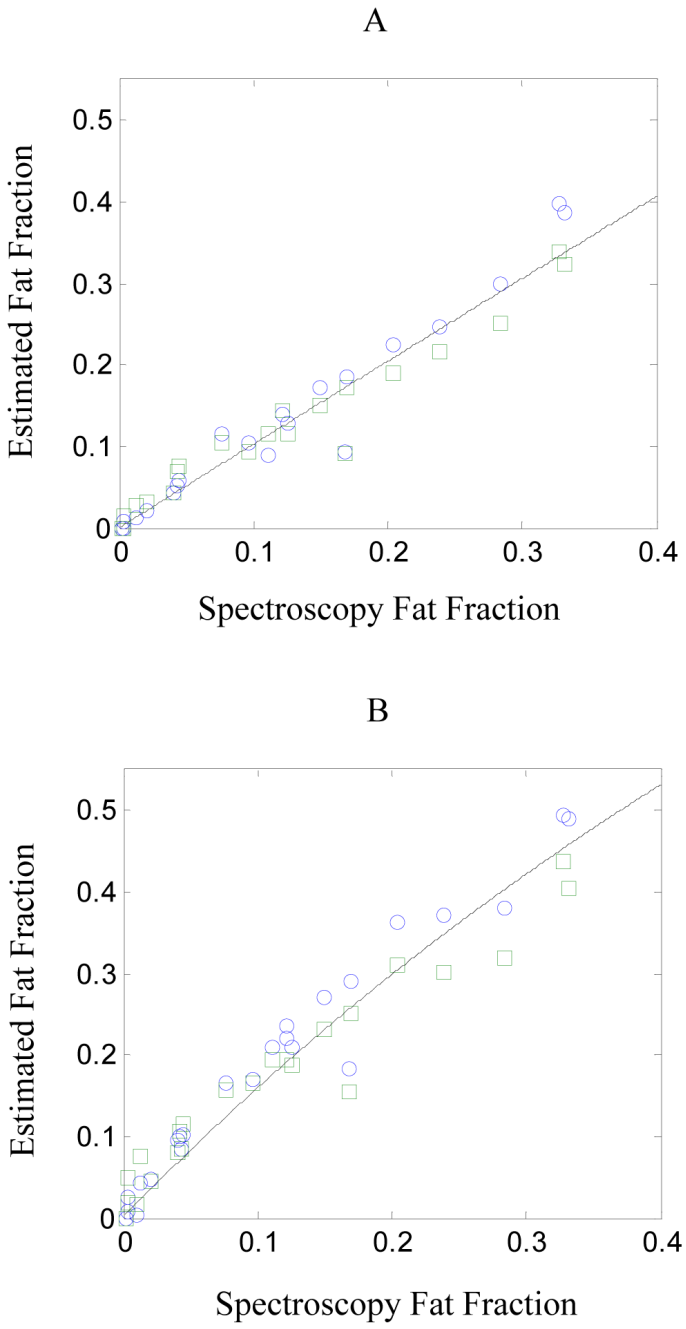

Figure 8.
Fat fractions determined by models (iv) and (v) using GRE imaging (circle and square markers, respectively) plotted against the fat fraction determined by spectroscopy using the STEAM sequence. Panel A shows the results using a flip angle of 10° and panel B shows the results using a flip angle of 90°. Assuming spectroscopy represents the true fat fraction, the solid lines show expected trends from Eq 9 with TR 122 ms, T1(water) = 490 ms and T1(fat) = 260 ms (24). Note the non-linearity due to T1-weighting is more evident in the high flip angle data.

Table I

A list of the symbols used in the present study

Symbol	Meaning
F	Fat Fraction
S	Total Signal
S_j	Signal of Component j
ω_j	Chemical Shift
v_j	R2 Relaxation Rate (1/T2)
v_{sys}	System R2 Relaxation Rate
v_j^*	R2* Relaxation Rate (1/T2*)
μ_j	R1 Relaxation Rate (1/T1)
ψ	Field Map
ϕ	Phase Offset
t	Echo Time (TE)
T	Repetition Time (TR)
α	Flip Angle

Table II

Abundance and T2 relaxation of the different fat peaks (relative to CH2 peak area) determined by spectroscopy in Intralipid (20 % fat fraction) and in 21 patients with fatty liver (various fat fractions). All amplitudes are corrected for T2 decay by taking spectra at multiple TE and curve-fitting the value to a TE of zero. Note the errors in the patient data reflect the standard deviation over the population and not error in the measurement

	0.8 - 0.9 ppm	**1.2 - 1.3 ppm**	**2.1 - 2.2 ppm**	**4.7 - 4.9 ppm**
Peak Area (Intralipid)	0.127	1.0	0.205	4.85
Peak T2 (Intralipid)	67.0 ms	51.7 ms	67.0 ms	802.9 ms
Peak Area (patient)	0.29 ± 0.12	1.0	0.18 ± 0.14	10.6 ± 8.0
Peak T2 (patient)	62 ± 163 ms	74.8 ± 19.2 ms	45.8 ± 29.8 ms	36.2 ± 4.9 ms

Table III

T2, T2* and T1 relaxation values in the phantom for the three doping conditions. Parentheses indicate the value was a fixed parameter in the model. High values for the T2* up to 500 are likely poorly estimated as the TE range was too small for a T2* of this value to exhibit any significant change

Model	*Gadolinium*		*None*		*Ferumoxides*	
	$\left(\nu_1^*\right)^{-1}$ (ms)	ν_2^{-1} (ms)	$\left(\nu_1^*\right)^{-1}$ (ms)	ν_2^{-1} (ms)	$\left(\nu_1^*\right)^{-1}$ (ms)	ν_2^{-1} (ms)
(i)	-	-	-	-	-	-
(ii)	-	(12)	-	(12)	-	(12)
(iii)	500	-	500	-	13.4	-
(iv)	299	(12)	360	(12)	13.1	(12)
(v)	280	10.4	369	9.5	13.0	6.3
(vi)	218	11.2	200	11.1	13.4	5.7
	μ_1^{-1} (ms)	μ_2^{-1} (ms)	μ_1^{-1} (ms)	μ_2^{-1} (ms)	μ_1^{-1} (ms)	μ_2^{-1} (ms)
(vi)	483	191	1830	166	144	115

Table IV

Best-fit values for the fat fraction are shown for models (i), (iii), (iv) and (v) in fatty liver during the course of a ferumoxides infusion. Also shown are the T2* parameters obtained from model (v). Note the system T2* $\left(\nu_{sys}^{-1}\right)$ should decrease considerably as the iron uptake increases in the liver while the fat fraction should remain constant

Time (min)	% F (model i)	% F (model iii)	% F (model iv)	% F (model v)	ν_{sys}^{-1} (ms)	ν_{2}^{-1} (ms)
0	17.4	17.3	24.6	24.3	24.6	12.5
5	17.3	17.6	24.8	24.3	21.7	12.9
10	17.3	18.2	25.4	24.9	18.3	12.9
15	16.6	18.4	25.4	25.5	15.3	11.8
20	15.2	18.3	25.1	24.7	13.0	12.7
25	14.0	18.3	24.8	24.4	11.4	12.8
30	13.9	19.3	25.7	24.8	9.8	13.8

Table V

Error calculated from Eq 12 between the fat fractions measured in 21 research subjects with fatty liver using spectroscopy and various models of the signal variation with TE from GRE imaging. Model (v) appears the most accurate

	Model (i)	**Model (ii)**	**Model (iii)**	**Model (iv)**	**Model (v)**	**Model (vi)**
Error	7.2	6.2	4.3	3.1	2.4	3.5

Magn Reson Imaging. Author manuscript; available in PMC 2009 April 1.